THE JOURNAL OF PHYSICAL CHEMISTRY A

Article

Cite This: J. Phys. Chem. A 2019, 123, 4274−4283

pubs.acs.org/JPCA

Bond Fragility Spectra for the Double Proton-Transfer Reaction in the Formic Acid-Type Dimers

Jarosław Zaklika,[†] Ludwik Komorowski,[†] and Piotr Ordon*[,‡]

[†]Department of Physical and Quantum Chemistry, Wrocław University of Science and Technology, Wyb. Wyspiańskiego 27, 50-370 Wrocław, Poland

[‡]Department of Physics and Biophysics, Wrocław University of Environmental and Life Sciences, ul. Norwida 25, 50-373 Wrocław, Poland

Supporting Information

ABSTRACT: The newly developed method of fragility spectra for observation of bond breaking and formation upon a reaction has been applied to the canonical reaction series of the double proton transfer (DPT). Formic acid and its thio-analogues HC**XY**H (**X**, **Y** = O, S) have been chosen for the analysis. Very accurate linear correlations have been determined between the nondiagonal elements of the connectivity matrix, essential for the method, and the Wiberg bond orders for the corresponding bonds. Relation of the slope of this correlation to the global softness and to the atomic numbers of the bonded atoms has been proved, thus corroborating the c-DFT formula describing the fragility spectra. The electron density changes in bonds, as observed by the fragility spectra, are in harmony with the curvature diagrams reported by other authors.

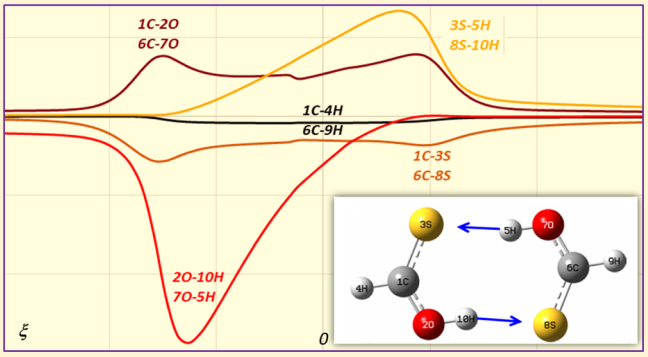

1. INTRODUCTION

The wide use of computational methods in theoretical studies for chemical kinetics has resulted in separation of the field into a number of specific goals, as recently reviewed by Klippenstein et al.[1] Detailed studies of the chemical dynamics are only possible, when the mechanism of the process is understood first.[2] The specific area of modern theory, which is aimed for understanding the chemistry, rather than reproducing the experimental data, has been opened by the advent of the conceptual density functional theory (c-DFT), as outlined by Parr[3] and his followers.[4−9] This specific theory is built around the electron density function $\rho(\mathbf{r})$ as it contains (in principle) adequate information for determination of the ground-state properties and on transformation of molecules, in a way similar to chemical thermodynamics. This has been symbolized by the central quantity of the c-DFT introduced by Parr: spatially equalized parameter of the chemical potential of electrons (μ), identified with the electronegativity ($-\chi$) crucial quantity in chemical practice.[10] Forty years later, Liu provided the significant assessment of the challenges in this field:[11] "even though modern computational chemistry is well established from the perspective of accuracy and complexity, how to quantify these chemical concepts is a still unresolved task."

An important contemporary chapter in bridging theory to chemical concepts has been opened by the advent of visualization techniques. Outlining the atomic orbitals has probably been the first step on this path: even an inaccurate picture reveals the fertile ground of the theoretical concept. The progress of the theory calls for exploration of such a method for the analysis of the subtle details of the reaction mechanism. According to Peters: visualizing the atom-by-atom contributions to progress along accurate and inaccurate reaction coordinates will help to train our intuition and thereby foster the discovery of new and perhaps simpler ways to understand mechanisms of complex reaction processes.[12]

The old idea of the transition state (TS) extended to identification of other stationary states on the potential energy surface represented the first step in this direction and has been widely appreciated by the chemical community. Notable progress was achieved by introduction of the intrinsic reaction coordinate (IRC),[13,14] exploring the normal modes, the necessary and ingenious concept for understanding the vibrational spectra and the reaction path itself.

The basics of IRC originate from adiabatic approximation that separates slow classical motion along the reaction path from fast vibrations described by quantum mechanics. Energy variations are given by the IRC Hamiltonian that incorporates terms responsible for mode mixing and mode switching. Modes are being mixed along the reaction path in terms of energy and bond breaking and forming. Coriolis coupling coefficients reflect this within the IRC theory. The switching of

Received: January 20, 2019
Revised: April 20, 2019
Published: April 22, 2019

DOI: 10.1021/acs.jpca.9b00595
J. Phys. Chem. A 2019, 123, 4274−4283

modes takes place because of the fact that bond-breaking mode pattern is eventually replaced by other bond-forming mode patterns. This is reproduced in adiabatic IRC theory by the set of curvature coefficients.[15] Observation of the reaction path curvatures provides in principle the complete picture of the reaction in terms of energy, with only indirect hints to the role of atoms and bonds, participating in the modes that are active in the process. This is a consequence of the founding principle:[16,17] separation of the vibrational energy into normal modes, despite the inconvenience of losing the chance to observe the reacting atoms.

Exploration of the vibrational modes for the description of the consecutive steps on IRC has been pursued in the important work by Cremer, Kraka et al.[18−22] The authors have introduced the unified reaction valley approach and the concept of the adiabatic internal vibrational mode (AIMO).[23] This is an elementary vibrational stretching mode tentatively exposed to describe a molecular fragment, typically a bond. Adiabatic modes are based on a dynamic principle, and they comply with the symmetry of the molecule. The concept has been used by the group to trace the chemical changes in a reacting system of atoms, that is, the bond forming and breaking as reflected by altering molecular normal modes. The basic point of their observation was the scalar curvature of the reaction path. Its decomposition into adiabatic curvature coefficients tentatively assigned to bonds allows for observation of the chemical changes in the reaction complex with the reaction progress. Independently, also Loerting studied in detail the coupling between the curvature of stretching modes and the minimum reaction path for the specific reaction of the double proton transfer (DPT).[24] The adiabatic stretching force constants calculated within the AIMO scheme were found to be related to the bond order, bond length, and the density at the critical point of the corresponding bond.[25] The final, most interesting result has been demonstrated by a diagram, showing the development of the energy curvature with the reaction progress and its decomposition into the contribution from individual modes, assigned to bonds, according to a leading component of a mode.[26] An impressive picture revealed four phases of the reaction, where the prevailing modes led to separated effects: reactant preparation (1), TS forming (2) and decay (3), and product adjustment (4). The authors noted how their achievements are related to the results of Toro-Labbé et al.[27] and Politzer et al.[28] who have argued independently for decomposition of the reaction path into three phases, limited by the extreme points of energy derivatives over the reaction progress: reaction force $F_\xi = -E^{(\xi)}$ and reaction force constant $k_\xi = E^{(\xi\xi)}$. This less sophisticated scheme does not require obtaining (diagonalized) Hessian matrix at each step of the reaction path.

2. THEORETICAL FRAMEWORK

We have recently published a study aimed at deciphering the bond formation and breaking process by means of a computational method, leading to the much needed visualization for the chemical use.[29,30] Unlike the former efforts concentrated on the vibrational modes, the focus of our work was on atoms, pointed by the Hellmann−Feynman (H−F) force acting upon them.[31] This way we avoid the main drawback of the vibrational approach, that is, having all the atoms involved in each step of the process.

The H−F force acting on a nucleus represents an effect of the electron density function in the entire system $\rho(\mathbf{r})$ and identifies each atom with no partition in the electron density[32]

$$-\nabla_A E = \mathbf{F}_A + \mathbf{F}_A^{n-n} \tag{1}$$

$\mathbf{F}_A$ uniquely contains the effect of the electron density on a single nucleus

$$\mathbf{F}_A = \int \rho(\mathbf{r})\varepsilon_A(\mathbf{r})\mathrm{d}\mathbf{r} \tag{2}$$

The internuclear interactions are separated in $\mathbf{F}_A^{n-n}$

$$\mathbf{F}_A^{n-n} = \sum_{B\neq A}^{\text{atoms}} Z_B \varepsilon_A(\mathbf{R}_B) \tag{3}$$

Although the electron density function $\rho(\mathbf{r})$ in the integral (eq 2) spans the whole system, the force $\mathbf{F}_A$ is dominated by the contribution from the density around a chosen nucleus because of the effect of its decreasing electric field (eq 4).

$$\varepsilon_A(\mathbf{r}) = -\nabla_A v(\mathbf{r}) = -Z_A \frac{(\mathbf{r} - \mathbf{R}_A)}{|\mathbf{r} - \mathbf{R}_A|^3} \tag{4}$$

Variations of the electron density function $\rho(\mathbf{r})$ occurring in a reaction result in the corresponding variations of the H−F force on atoms affected by this process. An important feature of the analysis, essential for the goals of this work, stems from the electrodynamical property of internuclear force vector $\mathbf{F}_A^{n-n}$

$$\nabla_A \cdot \mathbf{F}_B^{n-n} = 0 \tag{5}$$

This direct consequence of the Laplace equation[33] can be verified by calculating the divergence of the internuclear repulsion force, as specified by Yamaguchi et al.[34] The second derivative of energy (eq.1) equal to the divergence of H−F force contains the electronic contributions exclusively

$$-\nabla_A{}^2 E = \nabla_A \cdot \mathbf{F}_A \tag{6}$$

The divergence of force is a combination of elements of the common Hessian matrix. Hence, this concept has opened interesting prospects for observation of the electron density modifications upon a reaction. The density change around an atom in question must be reflected by the derivative[29,30]

$$a_\xi^A \equiv \frac{\mathrm{d}}{\mathrm{d}\xi}(\nabla_A \cdot \mathbf{F}_A) \tag{7}$$

a_ξ^A in eq 7 represents the third derivative of energy and belongs to the family of anharmonicity coefficients (cubic force constants).[35] It describes the effect of the reaction progress (ξ) on the force constant of the link of an atom with the entire electronic systems it belongs to (cumulative force constant). Consequently, the term fragility, used in other branches of chemistry, has been proposed for this quantity[29] (eq 7). Theoretical arguments based on the formalism of the c-DFT theory have been provided, indicating the approximate dependence of a_ξ^A on the density change $\mathrm{d}\rho(\mathbf{r})/\mathrm{d}\xi \neq 0$ on the reaction steps.[36] Indeed, the correlation between a_ξ^A and the derivative of valence of the corresponding atom variable on the IRC has been determined.[37] Observation of the atomic fragility (eq 7) along the reaction path provides a "spectrum" or a profile of changes reflecting the density evolution in bonding regions of an atom in question.[29,30]

This present work is aimed to extend the fragility concept to bonds between atoms. The key element of the analysis is the

DOI: 10.1021/acs.jpca.9b00595
J. Phys. Chem. A 2019, 123, 4274−4283

connectivity matrix ($n \times n$) defined for each point of the reaction path along the minimum energy coordinate.[30]

$$\underline{\underline{C}} = \begin{bmatrix} \nabla_A \cdot \mathbf{F}_A & \nabla_A \cdot \mathbf{F}_B & \dots & \nabla_A \cdot \mathbf{F}_N \\ \nabla_B \cdot \mathbf{F}_A & \nabla_B \cdot \mathbf{F}_B & \dots & \dots \\ \dots & \dots & \dots & \dots \\ \nabla_N \cdot \mathbf{F}_A & \dots & \dots & \nabla_N \cdot \mathbf{F}_N \end{bmatrix} \tag{8}$$

Elements of the matrix are divergences of H−F forces acting on the nuclei (eq 6). They represent the cumulative force constants in the system and may be calculated by a combination of the elements of the Hessian. For atoms (diagonal elements of the matrix)

$$\nabla_A \cdot \mathbf{F}_A = \frac{\partial F_{A,x}}{\partial R_{A,x}} + \frac{\partial F_{A,y}}{\partial R_{A,y}} + \frac{\partial F_{A,z}}{\partial R_{A,z}} \equiv C_{AA} \tag{9}$$

The important feature of the connectivity matrix should not be overlooked here: although there is generally no way to decompose the energy itself into additive components from atoms, the divergences of H−F forces on atoms represent pure atomic contributions, and they are free from the internuclear repulsion components. The interatomic terms are calculated accordingly

$$\nabla_{B\neq A} \cdot \mathbf{F}_A = \frac{\partial F_{A,x}}{\partial R_{B,x}} + \frac{\partial F_{A,y}}{\partial R_{B,y}} + \frac{\partial F_{A,z}}{\partial R_{B,z}} \equiv C_{AB} \tag{10}$$

Equation 10 is general and does not specify the bonds: the interatomic elements C_{AB} are calculated for any pair of atoms. All elements of the connectivity matrix contain the electronic energy contributions exclusively. According to the classification of forces proposed by Nakatsuji, the leading term in the interatomic elements $\nabla_{B\neq A} \cdot \mathbf{F}_A$ is the exchange force that represents the attraction between nuclei and the electron density in the region between nuclei A and B.[38]

An important relation of the nondiagonal elements to the electron density function has been proved by the conceptual DFT analysis.[30]

$$[\nabla_{B\neq A} \cdot \mathbf{F}_A]_N = -\int\int \omega(\mathbf{r}, \mathbf{r}')\varepsilon_B(\mathbf{r}') \cdot \varepsilon_A(\mathbf{r}) d\mathbf{r} d\mathbf{r}' \tag{11}$$

where $\omega(\mathbf{r},\mathbf{r}')$ is the linear response function[39] and $\varepsilon_B(\mathbf{r}')$ and $\varepsilon_A(\mathbf{r})$ are the electric field vectors at points $\mathbf{r}'$ and $\mathbf{r}$, respectively. This relation (eq 11) is simplified using the exact result of the conceptual DFT and the Parr and Berkowitz formula[40]

$$\omega(\mathbf{r}, \mathbf{r}') = -s(\mathbf{r}, \mathbf{r}') + s(\mathbf{r})f(\mathbf{r}') \tag{12}$$

where $s(\mathbf{r},\mathbf{r}')$ stands for the softness kernel and $s(\mathbf{r})$ and $f(\mathbf{r}')$ are the local softness and Fukui function, respectively.[41] This yields the exact equation

$$[\nabla_{B\neq A} \cdot \mathbf{F}_A]_N = \int\int s(\mathbf{r}, \mathbf{r}')\varepsilon_B(\mathbf{r}') \cdot \varepsilon_A(\mathrm{r}) d\mathbf{r} d\mathbf{r}' - S\mathbf{\Phi}_A \cdot \mathbf{\Phi}_B \tag{13}$$

where $\mathbf{\Phi}_A$ and $\mathbf{\Phi}_B$ are nuclear reactivity vectors, rigorously defined in the conceptual DFT as the derivative of the chemical potential μ.[30,42−48]

$$\mathbf{\Phi}_A = \nabla_A \mu = \int f(\mathbf{r})\varepsilon_A(\mathbf{r}) d\mathbf{r} \tag{14}$$

For the sake of practical analysis of the result in eq 13, the local approximation proposed by Vela and Gazquez is useful (eq 15). The formula has been widely explored in analyses of the polarization effects on the electron density.[49−51]

$$s(\mathbf{r}, \mathbf{r}') \cong s(\mathbf{r})\delta(\mathbf{r} - \mathbf{r}') \tag{15}$$

This allows for transformation of eq 13 into more tractable form

$$[\nabla_{B\neq A} \cdot \mathbf{F}_A]_N = S\int f(\mathbf{r})\varepsilon_B(\mathbf{r}) \cdot \varepsilon_A(\mathbf{r}) d\mathbf{r} - S\mathbf{\Phi}_A \cdot \mathbf{\Phi}_B \tag{16}$$

where S is the global softness. The integral in eq 16 reveals the very interesting dependence of the divergence $[\nabla_{B\neq A} \cdot \mathbf{F}_A]_N$ on the reaction progress. Arguments have been provided that the global quantities S, $\mathbf{\Phi}_A$, $\mathbf{\Phi}_B$ show only moderate change along the reaction.[30]

Equation 16 may be simplified even further. The crude approximation for the Fukui function binds it to the electron density function via the electron gas approximation[3]

$$f(r) = \frac{\rho(r)}{N} \tag{17}$$

where N is the number of electrons in the system described by the electron density function $\rho(\mathbf{r})$. By combination of eqs 16 and 17, the following approximate result is obtained

$$[\nabla_{B\neq A} \cdot \mathbf{F}_A]_N \cong \frac{S}{N}\int \rho(\mathbf{r})\varepsilon_B(\mathbf{r}) \cdot \varepsilon_A(\mathbf{r}) d\mathbf{r} - S\mathbf{\Phi}_A \cdot \mathbf{\Phi}_B \tag{18}$$

The important meaning of eq 18 is exposed, when the derivative over the reaction progress is calculated, with the electrodynamical constraint[30] $d\varepsilon_A(\mathbf{r})/d\xi = 0$

$$\frac{d}{d\xi}[\nabla_{B\neq A} \cdot \mathbf{F}_A]_N \cong \frac{S}{N}\int \frac{d\rho(\mathbf{r})}{d\xi}\varepsilon_B(\mathbf{r}) \cdot \varepsilon_A(\mathbf{r}) d\mathbf{r} + G_{AB} \tag{19}$$

The integral in the approximate eq 19 is helpful for understanding the variation of the force divergence $[\nabla_{B\neq A} \cdot \mathbf{F}_A]_N$ with the reaction progress. It is directly dependent on two factors: the change in the electron density function and the scalar product of the field vectors. The regions slightly affected by the reaction step $\Delta\xi$ do not contribute to the integral ($d\rho(\mathbf{r})/d\xi \approx 0$). The largest contribution to the derivative in eq 19 is likely to come from the bonding region between atoms, where the electron density undergoes substantial change $d\rho(\mathbf{r})/d\xi \neq 0$, both vectors $\varepsilon_A(\mathbf{r})$ and $\varepsilon_B(\mathbf{r})$ retain significant value and their orientation is parallel. Variations of global parameters in eq 19 ($dS/d\xi$, $G_{AB} = -d(S\mathbf{\Phi}_A \cdot \mathbf{\Phi}_B)/d\xi$) have been discussed in detail elsewhere.[30] Although not a constant, they are only moderately varying with the reaction progress because they are dominated by the overall density around the nuclei. The rich dynamics over ξ exposed by the derivative $d[\nabla_{B\neq A} \cdot \mathbf{F}_A]_N/d\xi$ (eq 19) comes from $d\rho(\mathbf{r})/d\xi$ in the region limited by the product $\varepsilon_B(\mathbf{r}) \cdot \boldsymbol{\varepsilon}_A(\mathbf{r})$, which is largest in the space between nuclei only.[29,30,37]

Let the bond fragilities be, by definition,

$$a_\xi^{AB} \equiv -\frac{d}{d\xi}[\nabla_{B\neq A} \cdot \mathbf{F}_A]_N \tag{20}$$

The minus sign in eq 20 is arbitrary and is intended to make this definition parallel to the atomic fragility a_ξ^A (eq 7).[30] From the property of the connectivity matrix (eq 8), we have

$$\nabla_A \cdot \mathbf{F}_A = -\sum_{B\neq A} \nabla_B \cdot \mathbf{F}_A \tag{21}$$

DOI: 10.1021/acs.jpca.9b00595
J. Phys. Chem. A 2019, 123, 4274−4283

The lhs is positive for all atoms, and, consequently, most terms in the sum on the rhs are negative. The definition of bond fragilities in eq 20 produces numbers representing the decomposition of the fragility of an atom into contributions from bonds (or contacts) to all other atoms in the reacting system.

$$a_{\xi}^{A} = \sum_{B \neq A} a_{\xi}^{AB} \tag{22}$$

The reaction selected for the study was DPT in the formic acid dimer-type structures. This process involves only minor displacement of atoms, except the proton being shifted, and yet, the C−X and C−Y bonds in the HCXY backbone (X, Y = O, S) undergo considerable modification. By studying the whole series of dimeric structures containing oxygen and sulfur atoms, it is possible to discern between the symmetrical rearrangement with $\Delta E = 0$ and nonsymmetrical ones ($\Delta E \neq 0$) and analyze the role of oxygen and sulfur atoms.

The proton dynamics of the formic acid dimers has been a subject of numerous computational works.[52,53] Specific analyses of the reaction path for the target group have also been attempted. In the theoretical study by Jaque and Toro-Labbé,[54] the evolution of the conceptual DFT descriptors has been presented. The chemical potential of the system was found to be weakly affected, while the global hardness falls to a minimum at TS because for the reaction of this kind the TS should be the most reactive state.[55] Another attempt was due to Yepes et al.[56] The authors analyzed the energy derivatives over the reaction progress ξ: the reaction force and reaction force constant; the second energy derivative ($E^{(\xi\xi)}$) has been advocated as an indicator of the reaction synchronicity. When the two proton replacements are considerably nonsynchronous, $E^{(\xi\xi)}$ has two minima separated by a local maximum, otherwise only single minimum is found.

The reaction is specific as it lacks the typical phase of approaching reagents (van der Waals phase). Here, both the reactant state and the product state (PS) are equilibrium dimeric structures either identical or differing by their symmetry and/or content. By using the fragility analysis, it is possible to trace not only the bonds between vicinal atoms but also any other contacts between atoms. The links over the atomic bridges are of particular interest (X/Y)−C−(Y/X), (X/Y)−H−(Y/X); the interactions through space have also been studied (X/Y)H···H(X/Y).

For the sake of completeness, the additional study of isomerization of the thioformic acid proton migration inside a monomer (HCOSH) has also been presented. It allows for comparison of the resulting fragility spectra to the similar diagram of the curvatures presented for this reaction by Kraka and Cremer.[26]

3. COMPUTATIONAL DETAILS

Numerical results for the elements of the connectivity matrix have been obtained from the IRC energy profile reproduced by the standard procedure at the MP2 level using the 6-311++G(3df,3pd) basis set and the Gaussian 09 code.[57] The method delivers analytical force constants very accurately. The TS structures have been identified by means of the QST3 algorithm and confirmed by frequency calculations. There is exactly one negative frequency value for each TS. The reaction progress parameter (ξ) has been calculated in the mass-weighted coordinates with standard number around 150−200 points over each reaction path studied.[15] The Cartesian Hessian elements and the harmonic frequencies for the normal modes have been calculated separately using the geometry of the structures resulting from the IRC scheme. These frequencies also show correct behavior. There is either exactly one negative eigenvalue (for structures close to the TS) or none.

The formic acid dimer (**R1**) has been known to have a planar structure and so does the TS for the DPT in this dimer. The TS geometry of its sulfur analogue (**R3**) has been found to be nonplanar, with the 60.5° angle between the monomer planes; in the set of related dimers, this angle is systematically smaller with the decreasing number of sulfur atoms: **R7** (48.2°), **R4** (30.1°). The dihedral angle between the twisted monomer planes also decreases with the increasing distance between sulfur atoms: **R5** (14.1°).

4. RESULTS

4.1. Energy Analysis. Calculated TS energies (ΔE_{TS}) have been collected in Table 1 for all systems studied. Results are in general agreement with the data reported in earlier work by Jaque and Toro-Labbé from the Hartree−Fock calculations, although their results were on the average by approximately 14 kcal/mol systematically larger.[54] TS energy for the formic acid dimer in Table 1 (**R1**: 7.20 kcal/mol) is much closer to the one reported by Kim:[58] 8.94 kcal/mol, obtained with MP2/6-311+G(*d*,*p*) than to the one reported in ref 54: (17.93 kcal/mol, RHF/6-311G**).

Table 1. TS Energies ΔE_{TS} and Reaction Energy ΔE for the DPT in the Formic Acid-Type Dimer: $X_1 + HY_1$ and $X_2H + Y_2 \rightarrow X_1H + Y_1$ and $X_2 + HY_2$[a]

The dimer molecule in the reactant state	No	X_1	X_2	Y_1	Y_2	ΔE [kcal/mol]	ΔE_{TS} [kcal/mol]
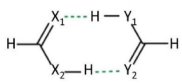	**R1**	O	O	O	O	0	7.20
	R2	S	S	O	O	0	12.46
	R3	S	S	S	S	0	11.34
	R4	O	S	O	S	0	10.80
	R5	S	O	O	S	1.59	13.67
	R6	O	S	O	O	-1.14	7.18
	R7	S	S	O	S	0.22	13.12

[a]Atoms losing the bond to a hydrogen are marked by shadow.

The collection of TS energies listed in Table 1 allows for attributing the individual energies for the proton shift between oxygen and sulfur atoms in these systems, assuming that the energy contributions from both moving protons are additive. Results and tests thereof have been collected in Table 2 (lhs). They are in harmony with the result reported by Turi for the single proton contribution to the TS energy in the formic acid dimer obtained with MP2/6-31++G(*d*,*p*)[59]

$$\Delta E_{TS}(O - H \rightarrow O = C) = 5.1 \div 5.4 \text{ kcal/mol}$$

$$\Delta E_{TS}(O - H \rightarrow O - C) = 2.7 \div 3.1 \text{ kcal/mol}$$

The estimated single proton contribution to the TS energy (Table 2, lhs) fairly well reproduces the original data (Table 2, rhs).

The critical test for the computational method is provided by the small reaction energy in nonsymmetrical systems (Table 1, **R5**, **R6**, **R7**). They meet expectation for the negative ΔE in

DOI: 10.1021/acs.jpca.9b00595
J. Phys. Chem. A 2019, 123, 4274−4283

Table 2. Calculated Individual Contributions to the TS Energy ΔE_{TS} from the Proton-Transfer Reaction [kcal/mol] and Cross-Test Thereof

type of proton motion	source	ΔE_{TS} for a single proton transfer ΔE_{TS} (H)	test: $\Delta E_{TS} = \Delta E_{TS}$ (H1) + ΔE_{TS}(H2)		
			reaction	original[b]	approx.
O−H → O	**R1**	3.60	**R4**	10.80	9.64
S−H → S	**R3**	5.67	**R7**	13.12	12.51
O−H → S	**R5**	6.84	**R2**	12.46	12.88
S−H → O	**R5**[a]	6.04	**R6**	7.18	7.52

[a]Reverse direction. [b]From Table 1.

R6, as compared to small, but positive ΔE in **R5**, **R7**. Calculation analogous to that presented above leads to the individual contribution to the reaction energy ΔE from one proton shift between different atoms O−H→S (from **R5**): 0.80 kcal/mol. The average estimation for a single proton shift energy (including **R5**, **R6**, and **R7**) is close to the result calculated from the data reported by other authors[54]

$$\Delta E(\mathrm{O-H} \rightarrow S) = 0.72 \pm 0.5\ \mathrm{kcal/mol}\ (\text{this work})$$

$$\Delta E(\mathrm{O-H} \rightarrow S) = 1.1 \pm 1.4\ \mathrm{kcal/mol}\ (\text{ref 54})$$

The energy diagrams for the DPT in two formic acid-type dimers $(HCOOH)_2$ and $(HCSSH)_2$ have been shown in the Supporting Information (Figure S1); the reaction force diagrams ($F_\xi = -dE/d\xi$) are also given.

4.2. Bond Fragility Spectra. Bond fragilities have been calculated according to definition (eq 20). Presentation of the results has been limited to the symmetric dimers (Figure 1). Fragility spectra for other dimers with the even number of heteroatoms in monomers and the nonsymmetric dimers have been presented in the Supporting Information (Figures S2 and S3).

The spectra in Figure 1 clearly disclose the repeated pattern for the bond fragility peaks of H−O and H−S bonds: the first is stronger than the latter, indicating the larger change in the electron density within the H−O bond in the process of its rupture (eq 19). The broad C−O and C−S fragility peaks tend to suggest a two-step change of these bonds, accompanying the two steps of the process: breaking of the O−H (S−H) bond well before TS and formation of new bonds after TS. The steep increase to an extreme (synchronous for atoms losing and gaining the hydrogen atom) for C−O (S−O) occurs already at the onset of the H−O (H−S) peak. Subsequent change is nearly stable until the final extreme. Peaks involving the sulfur atom are regularly less intensive than those for the oxygen atom.

4.3. Atomic Fragility Spectra. In order to confront the information between presented bond fragility spectra and analogous spectra for atoms, the atomic fragility spectra have been shown for two reactions **R1** and **R3** (Figure 2). They may be compared to the bond fragility spectra of the same species in Figure 1. The peak for a bond fragility (e.g., H−O) in Figure 1/**R1** and two peaks for the fragility of corresponding atoms (C, O) in Figure 2/**R1** appear in the same place on the ξ axis (ca. ±0.4). The same coincidence is observed for the H−S bond (Figure 2/**R3**) and the H, S atoms (Figure 1/**R3**) at $\xi \cong \pm 0.7$. This is consistent with the characteristics of these bonds: the H−S bond is considerably weaker and longer than H−O (136 and 96 pm, respectively).

4.4. Relation to Bond Orders. The nondiagonal elements of the connectivity matrix have been found to correlate with the Wiberg bond orders.[60] Meaningful correlations have been

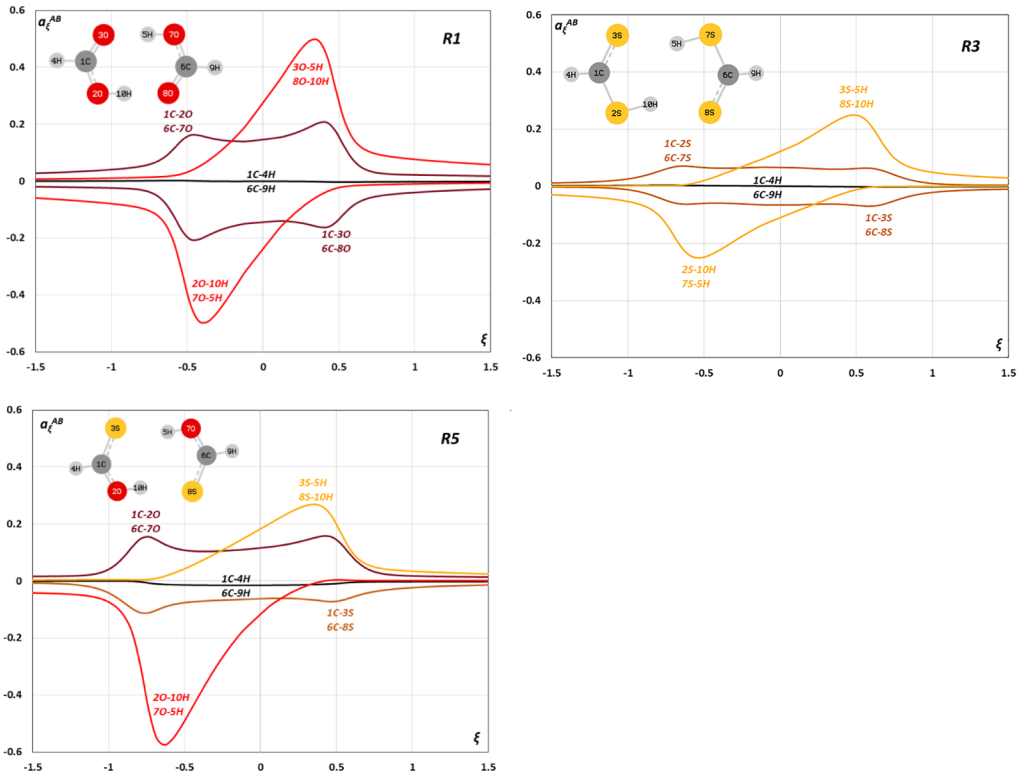

Figure 1. Bond fragility spectra (eq 20, a.u.) for the DPT in the symmetric dimers: **R1**, **R3**, **R5**. The spectra for both monomers strictly coincide.

DOI: 10.1021/acs.jpca.9b00595
J. Phys. Chem. A 2019, 123, 4274−4283

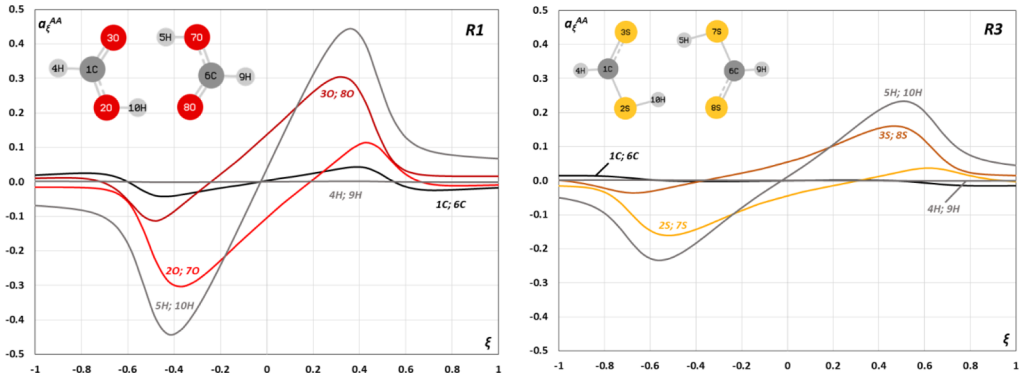

Figure 2. Fragility spectra (a.u.) for individual atoms as defined by eq 6 for two basic reactions **R1** and **R3**.

Table 3. Correlation Coefficients for the Empirical Linear Relation between the Wiberg Indices (W_{XY}) for Bonds and Corresponding Nondiagonal Elements of the Connectivity Matrix (C_{XY}): $W_{XY} = A\cdot[-C_{XY}] + B$ Calculated along the Entire Reaction Path [RS, PS]

monomer	softness[a] S	bond	A	B	number of molecules	average R^2
HCOOH	1.833	O−C(O)	1.60(±3)	0.18(±3)	6	0.9970(±2)
HCSOH	2.345	O−C(S)	1.96(±3)	0.024(±2)	5	0.9976(±1)
HCOSH	2.128	S−C(O)	2.95(±4)	0.38(±2)	5	0.9962(±1)
HCSSH	2.567	S−C(S)	3.75(±3)	0.12(±1)	6	0.9962(±4)

[a]Global softness calculated for the monomer as $S = (E_{LUMO} - E_{HOMO})^{-1}$ in [a.u.].

observed in the entire span of the reaction progress from the reagent state (RS) to the PS for bonds between heavy atoms (150 ÷ 200 points). Results are collected in Table 3. For the bonds to a moving proton, the correlation could only be observed for the halfway position, that is, [RS, TS] or [TS, PS], corresponding to the existence of the H−X bond (Table 4). For the hydrogen bond contact to an atom H···Y, meaningful correlations were not observed; the Wiberg index is close to zero.

Table 4. Correlation Coefficients for the Empirical Relation between the Wiberg Indices (W_{HX}) for the H−X Bond and Corresponding Nondiagonal Elements of the Connectivity Matrix (C_{HX}): $W_{HX} = A\cdot[-C_{HX}] + B$[a]

H−X bond type	A	B	number of molecules	average R^2
O···H−O(COH) S···H−O(COH)	0.68(±2)	0.31(±1)	4	0.995(±4)
O···H−O(CSH) S···H−O(CSH)	0.69(±3)	0.30(±1)	4	0.994(±4)
O···H−S(COH) S···H−S(COH)	1.48(±9)	0.50(±3)	4	0.994(±2)
O···H−S(CSH) S···H−S(CSH)	1.53(±10)	0.48(±3)	4	0.987(±4)
H−O(CSH)	0.56	0.42	1	0.995
H−S(COH)	0.96	0.68	1	0.998

[a]Correlations Cover the Range of Existence of bonds: [RS, TS] or [TS, PS].

The spectra of the very interesting direct bond of hydrogen to carbon atom (H−C) existing in all monomers studied has not been included in correlations. The correlation is clearly observed here beyond the TS region. However, because of the minute variation of both W_{CH} and C_{CH}, the data are less accurate than those presented for other bonds.

4.5. Fragility Spectra for Bonds and Atoms in HCOSH Isomerization. The HCOSH molecule isomerization has served as an example in the work by Kraka et al. (ref 26) in the analysis of AIMOs. The energies calculated for this reaction in this present work are as follows: $\Delta E_{TS} = 30.6$ and $\Delta E = -1.02$ [kcal/mol]. They reproduce the ones reported by other authors, respectively: 31.3 and −1.4 (B3LYP/6-311G/d.p/);[26] 32.8 and −1.43 (B3LYP/6-31G**).[61] The fragility spectra for this system provide complementary description of its atoms (Figure 3a) and bonds (Figure 3b). The upward peaks denote bond formation. The downward peaks come from the bond breaking. Peaks for atoms are grouped in pairs (Figure 3a) corresponding to a single bond peak (Figure 3b); this is observed clearly for the O−H bond breaking and S−H bond formation. The effect of strengthening the C−O bond and weakening the C−S bond is much better observed on the bond fragilities (Figure 3b).

The diagrams in Figure 3 contain demarcation of the borderlines between the reaction phases, as proposed by Kraka[26] for the reaction phases, and also the limits marked by the extremes of the reaction force.

4.6. Exploring the Correlation Parameters. The linear correlation established for the relation between the Wiberg bond indices W_{XY} and the elements of the connectivity matrix C_{XY} allows for testing the a priori derived relation (eq 16). Empirical correlation means that a linear function exists that binds W_{XY} with the only variable in eq 16 (the integral), other factors being approximately constant.

$$W_{XY} = A_{XY}\cdot[-\nabla_{X\neq Y}\cdot\mathbf{F}_Y]_N + B_{XY} = a_M(S_M Z_X Z_Y)\theta_{XY} + a_M S_M \mathbf{\Phi}_X\cdot\mathbf{\Phi}_Y \quad (23)$$

The integral θ_{XY} is formally defined as (eq 16)

$$\theta_{XY} = -\int \frac{(\mathbf{r} - \mathbf{R}_X)\cdot(\mathbf{r} - \mathbf{R}_Y)}{|\mathbf{r} - \mathbf{R}_X|^3|\mathbf{r} - \mathbf{R}_Y|^3} f(\mathbf{r})\mathrm{d}\mathbf{r} \quad (24)$$

DOI: 10.1021/acs.jpca.9b00595
J. Phys. Chem. A 2019, 123, 4274−4283

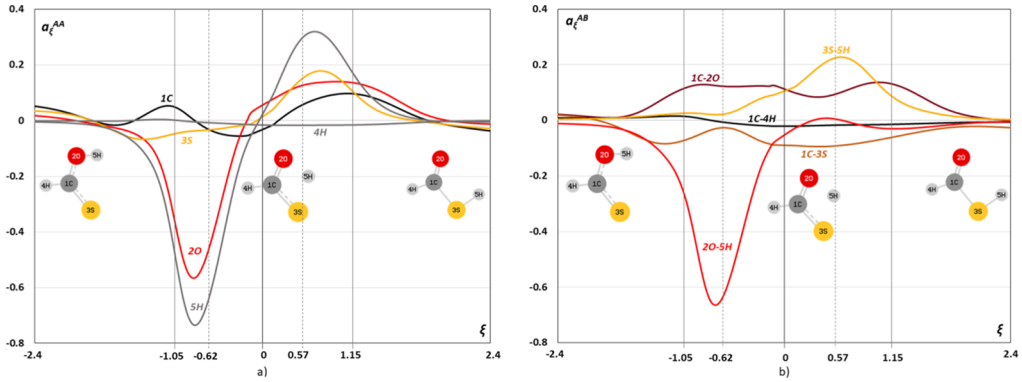

Figure 3. Fragility spectra (a. u.) for atoms (a) and bonds (b) in the HCOSH isomerization. The vertical lines mark the reaction phase limits as reported by Kraka [−1.05; 0, 1.15];[26] the dashed lines mark the position of the calculated extremes of the reaction force [−0.62, 0.57].

Hence, the slope (A_{XY}) of the correlation involving a bond X−Y (eq 23) in a monomer M may be checked, if it meets the requirement: $A_{XY} = a_M S_M Z_X Z_Y$, where a_M is the normalization parameter because the actual value of the integral is unknown. The quick test is possible from the data in Table 3 by comparing the ratio of the calculated slope for a pair of bonds (A in Tables 3 and 4) with the ratio of slopes $p = a_M(S_M Z_X Z_Y)$ as in the second part of eq 23 calculated for this pair of bonds, given the atomic numbers of partners and the softness of monomers.

$$\frac{A_1}{A_2} \cong \frac{p_1}{p_2} \tag{25}$$

When the pair belongs to the same molecule (monomer), it will have the same softness parameter S_M, otherwise calculated softness has been used (Table 3). There are no expectations for parameter a_M, except that it is unique for a molecule and possibly also for the collection of isostructural molecules because the slope A was found identical for the same bond in all reactions (Table 4). It appears to be dependent on the type of reaction, though, as the correlation parameters are not identical for the same bond in DPT and in the HCOSH. Results have been collected in Table 5. The data in Table 5 show reasonable coincidence between the calculated ratio A_1/A_2 and the expectation values estimated from p_1/p_2 (eq 25).

Similar considerations for parameter B on the linear correlation are less conclusive, though more interesting from the chemical point of view. They allow for estimation of the nuclear reactivity parameter in the reacting system $\mathbf{\Phi}$, representing the derivative of the chemical potential μ over displacement of a nucleus (eq 14). Equation 23 suggests possible relation for a X−Y bond in a monomer M.

$$B_{XY(M)} = a_M S_M \mathbf{\Phi}_X \cdot \mathbf{\Phi}_Y \tag{26}$$

The scalar product of the nuclear reactivities for vicinal atoms X, Y in a monomer M can thus be calculated for each molecule (eq 27). Numerical estimation of the products has been given in Table 6. Results are coherent with the first estimations of the nuclear reactivities for a series of diatomic molecules; however, the results of the present work are insufficient for determination of the vectors $\mathbf{\Phi}_X$, $\mathbf{\Phi}_Y$ themselves.[43]

$$(\mathbf{\Phi}_X \cdot \mathbf{\Phi}_Y)_M = \frac{B_{XY/M}}{A_{XY/M}} Z_X Z_Y \tag{27}$$

Table 5. Calculated Ratios of the Slope A in $W_{XY} = A\cdot[-C_{XY}] + B$ and of the $p = a_M(S_M Z_X Z_Y)$ Terms (eq 23) for Selected Pairs of Bonds[a]

bond 1	bond 2	A_1/A_2	p_1/p_2
O−C(S)	O−C(O)	1.22(±4)	1.28
S−C(S)	S−C(O)	1.28(±3)	1.20
S−C(O)	O−C(O)	1.83(±7)	2.32
S−C(S)	O−C(S)	1.92(±4)	2.18
H−S(COH)	H−O(COH)	2.17(±0.09)	2.32
H−S(CSH)	H−O(CSH)	2.21(±0.11)	2.19
H−S(COH)/M	H−O(CSH)/M	1.71	2
H−O(CSH)/M	H−O(CSH)/D	0.81	$a_{monomer}/a_{dimer}$
H−S(COH)/M	H−S(COH)/D	0.65	$a_{monomer}/a_{dimer}$

[a]The data are for the bonds in dimers, if not otherwise specified. The ratios for bonds in a monomeric HCOSH (M) and between bonds in the monomer (M) and in a dimer (D) have also been provided

Table 6. Calculated Scalar Products of the Nuclear Reactivity Vectors for Vicinal Atoms of the Bonds[a]

monomer	bond X−Y and $\mathbf{\Phi}_X\cdot\mathbf{\Phi}_Y$ [a.u.]					
HCOOH	H−O	3.65	O−C	5.40	C−O	5.40
HCSOH	H−O	3.48	O−C	0.59	C−S	12.4
HCOSH	H−S	5.40	S−C	12.4	C−O	0.59
HCSSH	H−S	5.02	S−C	3.07	C−S	3.07

[a]Calculated from the correlation parameters determined for the DPT process (eq 27)

5. DISCUSSION

Confrontation to the fragility spectra for bonds presented in Figure 3b and the result by Kraka et al. in their curvature diagram for the same reaction[26] provides an opportunity to evaluate the common features of the two methods. The general observation is that the curvature effects start much earlier (ca. $\xi \cong -2.5$) than the density deformation in bonds ($\xi \cong -1.5$) observed in fragility spectra. The O−H rupture is equally well described by curvature[26] (K2, $\xi \cong -0.8$) and by a strong negative peak in the fragility spectrum (2O−5H, $\xi \cong -0.7$). Also, the S−H bond formation is clearly visible on both

DOI: 10.1021/acs.jpca.9b00595
J. Phys. Chem. A 2019, 123, 4274−4283

diagrams[26] (K3 at $\xi \cong +0.7$; 3S−5H at +0.6). The picture of C−O and C−S bonds is different on the two diagrams but by no means contradictory. On the fragility spectrum (Figure 3b), the strengthening of the C−O bond begins at $\xi \cong -1.1$ and is completed only around $\xi \cong +1.5$; losing the C−S bond order is parallel, though slightly less intensive. The curvature diagram shows positive effect for C−S at $\xi \cong -1.5$ and is negative for C−O at $\xi \cong -1.3$; in the final phase, the C−O effects are reversed (at $\xi \cong 1.5$), and the C−S effects are hardly seen.

As far as the reaction phases are concerned, the fragility spectra support the conclusion that most of the electron-transfer processes (bond formation) do not occur specifically at TS but rather in the central region around it. The central region, as delimited by the reaction force extremes, represents the global effect only, with no connection to the specific process (bond formation) that actually occurs.

Both types of diagrams cover the central region around the TS. It is interesting to consider their relation to the tunneling effect known to play a substantial role in proton migration that leads to deviation of the reaction path from the minimum energy path.[62,63] The consequence is that the central part of the IRC diagram vanishes (is not active). The broadness of that gap may be estimated using the data by Kim,[58] reported for the formic acid dimer, that tunneling lowers the barrier by ca. 3.5 kcal/mol (by 40%). Recalculating the energy to the reaction progress gap yields ($-0.52 < \xi < 0.63$), close to the boundaries of the reaction force extremes.

6. CONCLUSIONS

The reaction fragility spectra provide vital information on the details of the reaction mechanism—describe the sequence of bond formation and breaking when approaching the TS and upon relaxing to the PS. The ease of calculation of the fragility spectra and their high sensitivity in detecting the reaction effects are certainly an asset for chemistry, as the language of reacting atoms is most natural in chemistry. On the other hand, the curvature diagrams describe the role of particular vibrational modes on each stage of the IRC path. It should be stressed that both methods are based on the information provided by the Hessian matrix. We extract this information for atoms and bonds from fragility spectra. Combined fragility spectra for atoms and bonds provide a ready-to-use tool for imaging of the bond reorganization in a chemical reaction, very much in the spirit expressed by Langvay in his study on the bond orders along a reaction path: "the main purpose is [to] ... translate the complex information provided by an ab initio quantum chemical calculation to a transparent 'chemical' language without any additional effort."[64]

■ ASSOCIATED CONTENT

Supporting Information

The Supporting Information is available free of charge on the ACS Publications website at DOI: 10.1021/acs.jpca.9b00595.

> Energy and reaction force diagrams for **R1** and **R3**, fragility profiles for symmetric dimers: **R2** and **R4**, fragility profiles for the nonsymmetric dimers in **R6** and **R7**, and fragility spectra for the H···H contact between hydrogens within the two hydrogen bonds affected by the reaction (**R1**, **R2**, **R3**, **R4**), as compared to the fragility spectrum for the links between heteroatoms separated by a carbon (X−C−Y) or a hydrogen atom: X−H → Y (X, Y = O, S) (PDF)

■ AUTHOR INFORMATION

Corresponding Author

*E-mail: piotr.ordon@upwr.edu.pl.

ORCID

Piotr Ordon: 0000-0002-7136-0367

Notes

The authors declare no competing financial interest.

■ ACKNOWLEDGMENTS

This work was financed by a statutory activity subsidy from the Polish Ministry of Science and Higher Education for the Faculty of Chemistry of Wrocław University of Science and Technology ref. no. 0401/0121/18. The authors are indebted to prof. W. A. Sokalski for his hospitality at the MDMM-18 conference, where the results have been presented and discussed. The use of resources of Wrocław Center for Networking and Supercomputing is gratefully acknowledged (WCSS grant no. 249 and GW 036). The helpful remarks by a referee are gratefully acknowledged.

■ REFERENCES

(1) Klippenstein, S. J.; Pande, V. S.; Truhlar, D. G. Chemical Kinetics and Mechanisms of Complex System: A Perspective on Recent Theoretical Advances. *J. Am. Chem. Soc.* **2014**, *136*, 528−546.

(2) López, J. G.; Vayner, G.; Lourderaj, U.; Addepalli, S. V.; Kato, S.; deJong, W. A.; Windus, T. L.; Hase, W. L. A Direct Dynamics Trajectory Study of F^- + CH_3OOH Reactive Collisions Reveals a Major Non-IRC Reaction Path. *J. Am. Chem. Soc.* **2007**, *129*, 9976−9985.

(3) Parr, R. G.; Yang, W. *Density-Functional Theory of Atoms and Molecules*; Oxford University Press: Oxford, U.K., 1989.

(4) Geerlings, P.; De Proft, F.; Langenaeker, W. Conceptual Density Functional Theory. *Chem. Rev.* **2003**, *103*, 1793−1874.

(5) Chermette, H. Chemical Reactivity Indexes in Density Functional Theory. *J. Comput. Chem.* **1999**, *20*, 129.

(6) Ayers, P. W.; Parr, R. G. Variational Principles for Describing Chemical Reactions. Reactivity Indices Based on the External Potential. *J. Am. Chem. Soc.* **2001**, *123*, 2007−2017.

(7) Nalewajski, R. F. A Coupling Between the Equilibrium State Variables of Open Molecular and Reactive Systems. *Phys. Chem. Chem. Phys.* **1999**, *1*, 1037−1049.

(8) Nalewajski, R. F. Internal Density Functional Theory of Molecular Systems. *J. Chem. Phys.* **1984**, *81*, 2088−2102.

(9) Liu, S. Conceptual Density Functional Theory and Some Recent Developments. *Acta Phys.—Chim. Sin.* **2009**, *25*, 590−600.

(10) Parr, R. G.; Donnelly, R. A.; Levy, M.; Palke, W. E. Electronegativity: The Density Functional Viewpoint. *J. Chem. Phys.* **1978**, *68*, 3801−3807.

(11) Liu, S.; Zhang, X. Chemical Concepts from Density Functional Theory. *Acta Phys.—Chim. Sin.* **2018**, *34*, 563−566.

(12) Peters, B. Common Features of Extraordinary Rate Theories. *J. Phys. Chem. B* **2015**, *119*, 6349−6356.

(13) Fukui, K. The Path of Chemical Reactions - the IRC Approach. *Acc. Chem. Res.* **1981**, *14*, 363−368.

(14) Miller, W. H.; Handy, N. C.; Adams, J. E. Reaction path Hamiltonian for polyatomic molecules. *J. Chem. Phys.* **1980**, *72*, 99−112.

(15) Piela, L. *Ideas of Quantum Chemistry*; Elsevier: Amsterdam N. L, 2007.

(16) Wilson, E. B., Jr.; Decius, J. C.; Cross, P. C. *Molecular Vibrations*; Dover Publications: New York, USA, 1980.

(17) Cyvin, S. J. *Molecular Vibrations and Mean Square Amplitudes*; Elsevier: Amsterdam, NL, 1968.

(18) Konkoli, Z.; Kraka, E.; Cremer, D. Unified Reaction Valley Approach Mechanism of the Reaction CH_3+H_2 → CH_4+H. *J. Phys. Chem. A* **1997**, *101*, 1742−1757.

DOI: 10.1021/acs.jpca.9b00595
J. Phys. Chem. A 2019, 123, 4274−4283

(19) Konkoli, Z.; Cremer, D. New Way of Analyzing Vibrational Spectra. I. Derivation of Adiabatic Internal Modes. *Int. J. Quantum Chem.* **1998**, *67*, 1−9.
(20) Konkoli, Z.; Larsson, J. A.; Cremer, D. A New Way of Analyzing Vibrational Spectra. II. Comparison of Internal Mode Frequencies. *Int. J. Quantum Chem.* **1998**, *67*, 11−27.
(21) Konkoli, Z.; Cremer, D. A New Way of Analyzing Vibrational Spectra. III. Characterization of Normal Vibrational Modes in Terms of Internal Vibrational Modes. *Int. J. Quantum Chem.* **1998**, *67*, 29−40.
(22) Konkoli, Z.; Larsson, J. A.; Cremer, D. A New Way of Analyzing Vibrational Spectra. IV. Application and Testing of Adiabatic Modes Within the Concept of the Characterization of Normal Modes. *Int. J. Quantum Chem.* **1998**, *67*, 41−55.
(23) Cremer, D.; Wu, A.; Kraka, E. The Mechanism of the Reaction FH + $H_2C{=}CH_2$ → $H_3C{-}CFH_2$. Investigation of Hidden Intermediates with the Unified Reaction Valley Approach. *Phys. Chem. Chem. Phys.* **2001**, *3*, 674−687.
(24) Loerting, T.; Liedl, K. R. Toward, Elimination of Discrepancies between Theory and Experiment: Double Proton Transfer in Dimers of Carboxylic Acids. *J. Am. Chem. Soc.* **1998**, *120*, 12595−12600.
(25) Kraka, E.; Cremer, D. Characterization of CF Bonds with Multiple-Bond Character: Bond Lengths, Stretching Force Constants, and Bond Dissociation Energies. *ChemPhysChem* **2009**, *10*, 686−698.
(26) Kraka, E.; Cremer, D. Computational Analysis of the Mechanism of Chemical Reactions in Terms of Reaction Phases: Hidden Intermediates and Hidden Transition States. *Acc. Chem. Res.* **2010**, *43*, 591−601.
(27) Toro-Labbé, A.; Gutiérrez-Oliva, S.; Politzer, P.; Murray, J. S. Reaction Force: A Rigorously Defined Approach to Analyzing Chemical and Physical Processes, In *Chemical Reactivity Theory. A density functional Viewpoint.* Chattaraj, P. K., Ed.; CRC Press, Taylor & Francis Group: Boca Raton, U.S.A., 2009.
(28) Politzer, P.; Toro-Labbé, A.; Gutiérrez-Oliva, S.; Murray, J. S. Perspectives on the Reaction Force In *Advances in Quantum Chemistry*, Sabin, J. R., Brändas, E. J., Eds.; Elsevier: Amsterdam, N.L., 2012; Vol.*64*.
(29) Komorowski, L.; Ordon, P.; Jędrzejewski, M. The Reaction Fragility Spectrum. *Phys. Chem. Chem. Phys.* **2016**, *18*, 32658−32663.
(30) Ordon, P.; Komorowski, L.; Jedrzejewski, M. Conceptual DFT Analysis of the Fragility Spectra of Atoms along the Minimum Energy Reaction Coordinate. *J. Chem. Phys.* **2017**, *147*, 134109.
(31) Jędrzejewski, M.; Ordon, P.; Komorowski, L. Atomic Resolution for the Energy Derivatives on the Reaction Path. *J. Phys. Chem. A* **2016**, *120*, 3780−3787.
(32) Feynman, R. P. Forces in Molecules. *Phys. Rev.* **1939**, *56*, 340−343.
(33) Jackson, J. D. *Classical Electrodynamics*, 2nd ed.; John Wiley & Sons Inc.: New York, USA, 1975.
(34) Yamaguchi, Y.; Osamura, Y.; Goddard, J. D.; Schaefer, H. F., III *A New Dimension to Quantum Chemistry: Analytic Derivative Methods in ab Initio Molecular Electronic Structure Theory*; Oxford University Press: New York—Oxford, 1994.
(35) Komorowski, L.; Ordon, P. Anharmonicity of a Molecular Oscillator. *Int. J. Quantum Chem.* **2004**, *99*, 153−160.
(36) Ordon, P.; Komorowski, L. DFT Energy Derivatives and their Renormalization in Molecular Vibrations. *Int. J. Quantum Chem.* **2005**, *101*, 703−713.
(37) Zaklika, J.; Komorowski, L.; Ordon, P. Evolution of the Atomic Valence Observed by the Reaction Fragility Spectra on the Reaction Path. *J. Mol. Model.* **2019**, *25*, 134.
(38) Nakatsuji, H. Theory for a Molecule and Interacting Molecules. I. Concept and Illustrative Applications. *J. Am. Chem. Soc.* **1973**, *95*, 345−354.
(39) Geerlings, P.; Fias, S.; Boisdenghien, Z.; De Proft, P. Conceptual DFT: Chemistry from the Linear Response Function. *Chem. Soc. Rev.* **2014**, *43*, 4989−5008.
(40) Berkowitz, M.; Parr, R. G. Molecular Hardness and Softness, Local Hardness and Softness, Hardness and Softness Kernels, and Relations Among these Quantities. *J. Chem. Phys.* **1988**, *88*, 2554−2557.
(41) Berkowitz, M.; Ghosh, S. K.; Parr, R. G. On the Concept of Local Hardness in Chemistry. *J. Am. Chem. Soc.* **1985**, *107*, 6811−6814.
(42) Cohen, M. H.; Ganduglia-Pirovano, M. V.; Kudrnovský, J. Electronic and Nuclear Chemical Reactivity. *J. Chem. Phys.* **1994**, *101*, 8988−8997.
(43) Ordon, P.; Komorowski, L. Nuclear Reactivity and Nuclear Stiffness in Density Functional Theory. *Chem. Phys. Lett.* **1998**, *292*, 22−27.
(44) De Proft, F.; Liu, S.; Geerlings, P. Calculation of the Nuclear Fukui Function and New Relations for Nuclear Softness and Hardness Kernels. *J. Chem. Phys.* **1998**, *108*, 7549−7554.
(45) Luty, T.; Ordon, P.; Eckhardt, C. J. A Model for Mechanochemical Transformations: Applications to Molecular Hardness, Instabilities, and Shock Initiation of Reaction. *J. Chem. Phys.* **2002**, *117*, 1775−1785.
(46) Baekelandt, B. G. The Nuclear Fukui Function and Berlin's Binding Function in Density Functional Theory. *J. Chem. Phys.* **1996**, *105*, 4664.
(47) Ordon, P.; Tachibana, A. Nuclear Reactivity Indices within Regional Density Functional Theory. *J. Mol. Model.* **2005**, *11*, 312−316.
(48) Ordon, P.; Tachibana, A. Investigation of the Role of the C-PCM Solvent Effect in Reactivity Indices. *J. Chem. Sci.* **2005**, *117*, 583−589.
(49) Vela, A.; Gazquez, J. L. A Relationship Between the Static Dipole Polarizability, the Global Softness, and the Fukui Function. *J. Am. Chem. Soc.* **1990**, *112*, 1490−1492.
(50) Komorowski, L.; Lipiński, J.; Szarek, P. Polarization Justified Fukui Functions. *J. Chem. Phys.* **2009**, *131*, 124120.
(51) Komorowski, L.; Lipiński, J.; Szarek, P.; Ordon, P. Polarization Justified Fukui Functions: The Theory and Applications for Molecules. *J. Chem. Phys.* **2011**, *135*, 014109.
(52) Qian, W.; Krimm, S. Origin of the CdO Stretch Mode Splitting in the Formic Acid Dimer. *J. Phys. Chem.* **1996**, *100*, 14602−14608.
(53) Qian, W.; Krimm, S. Electrostatic Model for the Interaction Force Constants of the Formic Acid Dimer. *J. Phys. Chem. A.* **1998**, *102*, 659−667.
(54) Jaque, P.; Toro-Labbé, A. Theoretical Study of the Double Proton Transfer in the CHX-XH...CHX-XH (X=O, S) Complexes. *J. Phys. Chem. A* **2000**, *104*, 995−1003.
(55) Ordon, P.; Tachibana, A. Use of Nuclear Stiffness in Search for a Maximum Hardness Principle and for the Softest States along the Chemical Reaction Path: A new Formula for the Energy Third Derivative γ. *J. Chem. Phys.* **2007**, *126*, 234115.
(56) Yepes, D.; Murray, J. S.; Politzer, P.; Jaque, P. The Reaction Force Constant: An Indicator of the Synchronicity in Double Proton Transfer Reactions. *Phys. Chem. Chem. Phys.* **2012**, *14*, 11125−11134.
(57) Frisch, M.; Trucks, G.; Schlegel, H.; Scuseria, G.; Robb, M.; Cheeseman, J.; Scalmani, G.; Barone, V.; Mennucci, B.; Petersson, G. *GAUSSIAN 09* (Revision A.02); Gaussian, Inc: Wallingford, CT, 2009.
(58) Kim, Y. Direct Dynamics Calculation for the Double Proton Transfer in Formic Acid Dimer. *J. Am. Chem. Soc.* **1996**, *118*, 1522−1528.
(59) Turi, L. Ab Initio Molecular Orbital Analysis of Dimers of *cis*-Formic Acid. Implications for Condensed Phases. *J. Phys. Chem.* **1996**, *100*, 11285−11291.
(60) Mayer, I. Bond Order and Valence Indices. *J. Comput. Chem.* **2007**, *28*, 204−221.
(61) Gutiérrez-Oliva, S.; Herrera, B.; Toro-Labbé, A.; Chermette, H. On the Mechanism of Hydrogen Transfer in the HSCH(O)↔(S)-CHOH and HSNO↔SNOH Reactions. *J. Phys. Chem. A* **2005**, *109*, 1748−1751.
(62) Miura, S.; Tuckerman, M. E.; Klein, M. L. An ab initio Path Integral Molecular Dynamics Study of Double Proton Transfer in the Formic Acid Dimer. *J. Chem. Phys.* **1998**, *109*, 5290−5299.

DOI: 10.1021/acs.jpca.9b00595
J. Phys. Chem. A 2019, 123, 4274−4283

(63) Shida, N.; Barbara, P. F.; Almlöf, J. A Reaction Surface Hamiltonian Treatment of the Double Proton Transfer of Formic Acid Dimer. *J. Chem. Phys.* **1991**, *94*, 3633−3643.
(64) Lendvay, G. Characterization of the Progress of Chemical Reactions by ab Initio Bond Orders. *J. Phys. Chem.* **1994**, *98*, 6098−6104.

DOI: 10.1021/acs.jpca.9b00595
J. Phys. Chem. A 2019, 123, 4274−4283